Agricultural and Forest Meteorology 275 (2019) 305–316

Contents lists available at ScienceDirect

Agricultural and Forest Meteorology

journal homepage: www.elsevier.com/locate/agrformet

Assessing consistency of spring phenology of snow-covered forests as estimated by vegetation indices, gross primary production, and solar-induced chlorophyll fluorescence

Qing Chang[a], Xiangming Xiao[a,*], Wenzhe Jiao[b], Xiaocui Wu[a], Russell Doughty[a], Jie Wang[a], Ling Du[a], Zhenhua Zou[a], Yuanwei Qin[a]

[a] Department of Microbiology and Plant Biology, Center for Spatial Analysis, University of Oklahoma, Norman, OK 73019, USA
[b] Department of Earth Sciences, Indiana University-Purdue University Indianapolis (IUPUI), Indianapolis, IN 46202, USA

ARTICLE INFO

Keywords:
Eddy flux tower sites
NDVI
EVI
LSWI
Temperature
Photosynthesis
MODIS

ABSTRACT

Accurate phenology characterization is of great importance for measuring ecosystem dynamics, especially for carbon and water exchange between land and the atmosphere. Vegetation indices (VIs), calculated from land surface reflectance, are widely used to estimate phenology from the leaf and canopy structure perspective. Gross Primary Production (GPP) and solar-induced chlorophyll fluorescence (SIF) are used to estimate phenology from the canopy functional (physiological) perspective. To what degree are the spring phenology estimated from these different perspectives consistent with each other? In this study, we evaluated the consistency of the start of the growing season (SOS) in spring for snow-covered evergreen needleleaf forests (ENF) and deciduous broadleaf forests (DBF) using three vegetation indices, *in-situ* GPP data from the eddy covariance flux towers (GPP_{EC}), GPP data from the Vegetation Photosynthesis Model (GPP_{VPM}), and SIF data from the GOME-2. Results showed that SOS_{NDVI} dates were much earlier than SOS dates from EVI (SOS_{EVI}), land surface water index (LSWI) (SOS_{LSWI}), GPP (SOS_{GPP}; $SOS_{GPP\text{-}EC}$, SOS_{GPP_VPM}) and SIF (SOS_{SIF}) for both snow-covered evergreen needleleaf forest (ENF) and deciduous broadleaf forest (DBF). SOS_{LSWI} dates were more linearly correlated with SOS_{GPP} and SOS_{SIF} than SOS dates from NDVI and EVI. At ENF sites, SOS_{LSWI} dates were 17 (± 27) days later and SOS_{EVI} were 25 (± 34) days later than SOS_{GPP_EC} dates. At DBF sites, SOS_{LSWI} and SOS_{EVI} dates were 1-week (± 13 days) later than SOS_{GPP_EC} dates. In the snow-covered regions at mid- to high-latitude in the Northern Hemisphere, SOS_{LSWI} dates were 2~3 weeks (± 5 days) later than those of SOS_{GPP_VPM} and SOS_{SIF} for both ENF and DBF. Our results clearly highlight the need for further investigation of NDVI-based SOS dates, which were likely affected by snowmelt in snow-covered forests, and the potential of LSWI for tracking the effects of snow on SOS dates. Estimations of SOS dates in snow-covered forests should consider the effects of both snow cover and temperature on leaf emergence (green-up) and gross primary production.

1. Introduction

Vegetation (leaf and canopy) phenology significantly affects carbon and water cycles (Hollinger et al., 1999; Peñuelas and Filella, 2009; Richardson et al., 2010) and is often characterized from the perspective of leaf and canopy structure (e.g., leaf flush, green-up) or from the perspective of leaf and canopy function (e.g., photosynthesis or gross primary production (Churkina et al., 2005; Ma et al., 2007; Piao et al., 2007; Richardson et al., 2010). Accurate measurements and the comparison of vegetation phenology from the structural and functional perspectives are significant for improving terrestrial models and exploring ecosystem carbon-water interaction and variability (Wu et al., 2012; Zhang et al., 2003).

Over the past decades, optical remote sensing has been used to identify vegetation phenology and land surface phenology (Matsumoto et al., 2003; Piao et al., 2007; Wu et al., 2013; Zhang et al., 2013). Vegetation indices (e.g., normalized difference vegetation index (NDVI), enhanced vegetation index (EVI), land surface water index (LSWI)) and leaf area index (LAI) provide information on the dynamics of canopy structure and are the primary indices used for estimating the start and end of the growing season (SOS, EOS) from the perspective of canopy structure (Hmimina et al., 2013; Sims et al., 2006; Xiao et al., 2004b; Zhang et al., 2003). The SOS dates estimated by the vegetation indices derived from the Moderate Resolution Imaging

* Corresponding author.
E-mail address: xiangming.xiao@ou.edu (X. Xiao).

https://doi.org/10.1016/j.agrformet.2019.06.002
Received 20 February 2019; Received in revised form 18 May 2019; Accepted 2 June 2019

Spectroradiometer (MODIS) varied among land cover types, soil moisture conditions, and even extreme climate events (Liu et al., 2016; Peng et al., 2017a; Shen et al., 2014b; Wu et al., 2014). Our understanding of the unique advantages of each vegetation index in estimating spring phenology and the differences among the VI-based indicators of phenology across vegetation types is still limited (Balzarolo et al., 2016; Chang et al., 2018; Reed et al., 2009).

Gross primary production (GPP) of forests (Baldocchi et al., 2001; Zhang et al., 2006) is also used for estimating SOS and EOS from the perspective of canopy function. Several studies reported that canopy structure phenology from satellites were consistent with the phenology from flux tower GPP observations (Balzarolo et al., 2016) and NEE (Wang et al., 2016), and the net carbon uptake period (CUP) from NEE has been widely used for validation of land surface phenology derived from satellite data analysis (Peng et al., 2017b; Verma et al., 2014; Xiao et al., 2008; Zhang et al., 2016b). However, some other studies reported that no single source of canopy phenology data was able to accurately describe annual patterns of phenology from the eddy flux GPP or NEE data, and the differences are inconsistent across vegetation types (Garrity et al., 2011; Wu et al., 2017). The contrary conclusions could have been caused by snow-cover at the selected sites, which was not addressed in these studies. Thus, further investigation into the consistencies and differences in satellite-based indicators of vegetation canopy structural and functional phenology is needed.

Solar-induced chlorophyll fluorescence (SIF) emitted by vegetation (Guanter et al., 2014; Sun et al., 2018; Wang et al., 2016) was recently used to estimate SOS and EOS from the perspective of canopy function (Joiner et al., 2014). SIF is a kind of photosynthesis-related energy and is directly detected by satellite sensor instead of being modeled based on indirectly satellite datasets (Joiner et al., 2013; Sun et al., 2018). Phenology studies of SIF can help us better understand seasonal dynamics of photosynthesis (Jeong et al., 2017; Walther et al., 2016) and to assess the uncertainties in modeled GPP products (Guanter et al., 2014; Wang et al., 2016). A number of studies have shown that GPP is closely related to SIF (Li et al., 2018; Walther et al., 2016; Zhang et al., 2016b). However, the relationship between GPP and SIF varies from the leaf scale to the canopy scale, and also depends on the time frame (diurnal, daily, seasonal) and biome type (Li et al., 2018; Zhang et al., 2016a). The consistency between the functional phenology metrics derived from GPP and SIF has not yet well studied. Furthermore, structure-based spring phenology dates derived from NDVI, EVI, and LSWI have not yet been compared with phenology from SIF. A comprehensive study is urgently needed for comparing the SOS dates from vegetation indices (NDVI, EVI, LSWI), GPP, and SIF.

Phenology studies in snow-covered deciduous and evergreen forests at mid- to high-latitude regions are complex because of snow cover (Botta et al., 2000; Julien and Sobrino, 2009; Zhang et al., 2006). SOS date estimates using vegetation indices are always biased by snow cover, which affects satellite reflectance (Chen et al., 2015; Delbart et al., 2006; Wang et al., 2017; Zhang, 2015). Decoupling the snowmelt signal from vegetative growth is essential for accurate phenology estimation. The effects of snow on spring phenology (SOS estimates) by vegetation indices, GPP, and SIF are not fully investigated. The consistency of spring phenology of snow-covered forests from the perspectives of canopy structure (VIs) and function (GPP, SIF) is not yet well known. Furthermore, as air temperature is the most important environmental factor controlling both SOS (Ensminger et al., 2004; Piao et al., 2015; Wang et al., 2015) and snowmelt processes (Groendahl et al., 2007), there is also a need to understand the effect of air temperature on vegetation indices, GPP and SIF, which would in turn affect their SOS estimates.

In this study, we investigated the consistency of SOS estimates of snow-covered evergreen needleleaf forests (ENF) and deciduous broadleaf forests (DBF) from the perspectives of canopy structure (vegetation indices) and function (GPP and SIF). We used two greenness-related vegetation indices (NDVI and EVI) and one water-related vegetation index (LSWI) from MODIS images, GPP data from the eddy flux tower sites (GPP_{EC}), GPP data from the Vegetation Photosynthesis Model (GPP_{VPM}), and SIF data from the GOME-2. We addressed the following questions: (1) what is the consistency of SOS dates from VIs (NDVI, EVI, and LSWI) and from GPP_{EC} at snow-covered ENF and DBF eddy flux tower sites? (2) what is the consistency of SOS dates from VIs (NDVI, EVI, and LSWI), GPP_{VPM}, and SIF at snow-covered ENF and DBF forests across the mid- to high-latitude North Hemisphere? (3) what are the responses of VIs, GPP, and SIF to daytime air temperature during the initial growth stage of snow-covered ENF and DBF? We first evaluated the consistency of SOS from vegetation indices (NDVI, EVI, and LSWI) and GPP (GPP_{EC}, GPP_{VPM}) at the site level using snow-covered forest flux tower observations, and then explored the consistency of SOS of snow-covered ENF and DBF from VIs, GPP_{VPM}, and SIF data at regional scale for snow-covered ENF and DBF in the mid- to high-latitude Northern Hemisphere. The relationships between various data sources and air temperature were also analyzed to show the reliability of SOS dates estimated from various datasets at snow-covered ENF and DBF sites.

2. Materials and methods

2.1. Study sites

We selected 17 forest eddy flux tower sites (8 ENF and 9 DBF sites) from the FLUXNET-2015 dataset (http://fluxnet.fluxdata.org/data/fluxnet2015-dataset/) (Table 1). Site selection was based on the following criteria: (1) sites must have more than 8 years of observations between 2000 and 2014; (2) sites are relatively homogeneous land cover within the pixels of the MODIS MOD09A1 product (500 m spatial resolution) (Fig. S.1); and (3) sites have snow cover in winter and spring, according to the site description and MODIS normalized difference snow index (NDSI). MODIS NDSI is calculated from green band and short wave infrared band, and is used to assess snow conditions. The MODIS snow-mapping algorithm identifies an observation as snow when NDSI value is equal to or greater than 0.4 (with more than 50% snow cover) (Hall et al., 1995, 2002; Zhang et al., 2003). In our study, only those years identified to have snow cover during the winter (previous December, January, and February) to spring (March, April, and May) for each site were used. For the flux towers listed in Table 1, years with no snow cover were removed. The removed years for the used sites include RU-Fyo (2005, 2008), DK-Sor (2003, 2004, 2007, 2008, 2012, 2014), DE-Hai (2004, 2005, 2007, 2008, 2009, 2012), FR-Fon (2005, 2007–2014), US-Wcr (2000, 2012), US-Ha1 (2000, 2002–2007, 2010–2012), IT-Col (2000–2002, 2007, 2008, 2011, 2012, 2014), and US-MMS (2000, 2002–2006, 2008, 2009, 2011–2013).

2.2. Data

2.2.1. Climate and GPP data from the CO_2 flux tower sites

The FLUXNET eddy covariance network measures ecosystem CO_2, heat fluxes, and meteorological variables at sites across the globe. The FLUXNET-2015 eddy covariance GPP (GPP_{EC}) datasets were calculated from gap-filled net ecosystem exchange (NEE) data using the standard flux-partitioning method (Lasslop et al., 2010). The GPP product (GPP_DT_VUT_REF) used in this study was calculated with the variable USTAR filtering approach and daytime partitioning method (Kumar et al., 2016). Daily GPP datasets were used in this study to determine SOS. Daily average daytime air temperature datasets (TA_F) from FLUXNET-2015 were also used to explore the relationship between temperature and phenology. Daily observations at the flux tower sites were aggregated to an 8-day and monthly temporal resolutions to match the MODIS VIs and GOME-2 SIF data, respectively.

2.2.2. MODIS surface reflectance data and vegetation indices

The MODIS surface reflectance product MOD09A1 V6 is provided

Table 1
Description of FLUXNET sites, Elevation, Annual temperature, precipitation, and Plant functional types (DBF-Deciduous broadleaf forest, ENF-Evergreen Needleleaf forest).

Site ID	Latitude (decimal degrees)	Longitude (decimal degrees)	Elevation (m)	Plant functional type	Mean annual Temperature (degree C)	Mean annual Precipitaion (mm)	Observed years
FI-Sod	67.3619	26.6378	180	ENF	−1	500	2001–2014
FI-Hyy	61.8475	24.295	181	ENF	3.8	709	2000–2014
RU-Fyo	56.4615	32.9221	265	ENF	3.9	711	2000–2014
CA-Man	55.8796	−98.4808	259	ENF	−3.2	520	2000–2008
CA-Qfo	49.6925	−74.3421	382	ENF	−0.36	962	2003–2010
CH–Dav	46.8153	9.8559	1639	ENF	2.8	1062	2000–2014
IT–Ren	46.5869	11.4337	1730	ENF	4.7	809	2000–2013
US–GLE	41.3665	−106.2399	3197	ENF	0.8	1200	2004–2014
US–NR1	40.0329	−105.5464	3050	ENF	1.5	800	2000–2014
DK–Sor	55.4859	11.6446	40	DBF	8.2	660	2000–2014
DE–Hai	51.0792	10.453	430	DBF	8.3	720	2000–2012
FR–Fon	48.4764	2.7801	103	DBF	10.2	720	2005–2014
US–WCr	45.8059	−90.0799	520	DBF	4.02	787	2000–2014
US–UMd	45.5625	−84.6975	239	DBF	5.83	803	2007–2014
US–UMB	45.5598	−84.7138	234	DBF	5.83	803	2000–2014
US–Ha1	42.5378	−72.1715	340	DBF	6.62	1071	2000–2012
IT–Col	41.8494	13.5881	1560	DBF	6.3	1180	2000–2014
US–MMS	39.3232	−86.4131	275	DBF	10.85	1032	2000–2014

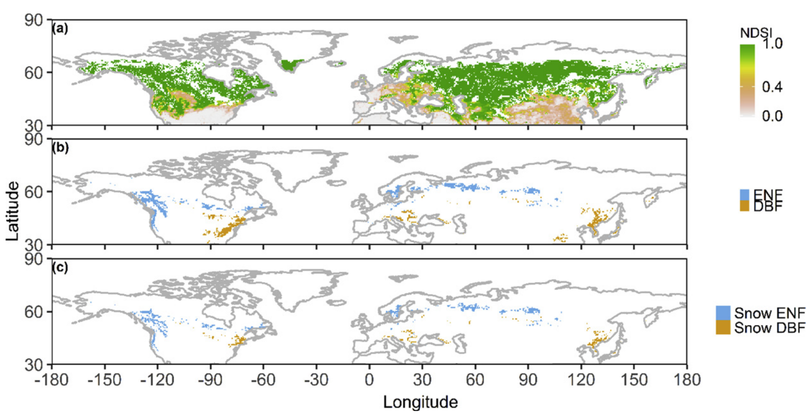

Fig. 1. Spatial distributions of (a) MODIS normalized difference snow index (NDSI) in January in 2010; (b) evergreen needleleaf forest (ENF) and deciduous broadleaf forest (DBF) from MODIS land cover product in 2010; and (c) snow-covered ENF (773 pixels) and DBF (334 pixels) (NDSI > 0.4) in mid- to high-latitudes of Northern Hemisphere.

with 500-m spatial resolution and 8-day interval temporal resolution (Vermote, 2015). The MOD09A1 dataset was used to calculate four spectral indices including NDSI (Hall et al., 1995, 2002), NDVI (Rouse et al., 1974), EVI (Huete et al., 2002), and LSWI (Xiao et al., 2004a) (see Eqs. (1)–(4)). MODIS bands were used in these equations including: red band (RED) (620–670 nm), near infrared band (NIR) (841–876 nm), blue band (BLUE) (459–479 nm), green band (GREEN) (545–565 nm), and short wavelength near infrared band (SWIR) (1628–1652 nm). NDSI was used to determine snow cover at 500-m spatial resolution. NDSI values for mid- to high-latitude NH are shown in Fig. 1 a.

Vegetation indices (NDVI, EVI, and LSWI) at the flux sites were calculated from MOD09A1-based bands reflectance products. Prior to calculating the phenology metrics, we processed the time-series VIs using the following three steps. First, observations affected by cloud cover were identified by using the quality assurance (QC) flags for cloud state ("00" flags indicate clear sky), and were gap-filled using the multi-year mean of good observations for that day. Second, we used the Best Index Slope Extraction (BISE) method to detect bad-quality observations unidentified in the QC layer in NDVI time series, and the bad observations were replaced with the mean value of its nearest two good observations (Viovy et al., 1992; White et al., 1997; Xiao et al., 2009). Third, we used the S−G filter method to remove abnormal values in the time series data (Chen et al., 2004; Savitzky and Golay, 1964).

$$NDSI = \frac{GREEN - SWIR}{GREEN + SWIR} \tag{1}$$

$$NDVI = \frac{NIR - RED}{NIR + RED} \tag{2}$$

$$EVI = 2.5 \times \frac{NIR - RED}{(NIR + 6 \times Red - 7.5 \times BLUE + 1)} \tag{3}$$

$$LSWI = \frac{NIR - SWIR}{NIR + SWIR} \tag{4}$$

2.2.3. GPP data from the VPM simulations

We used the GPP data product simulated from Vegetation Photosynthesis Model (VPM) (GPP_{VPM}) at 500-m spatial resolution. VPM estimates GPP as a function of photosynthetically active radiation (PAR) absorbed by chlorophyll ($APAR_{chl}$) and light use efficiency (ε_g) (Xiao et al., 2004a). Two basic equations for LUE-based VPM are shown as Eqs. (5) and (6). The global GPP_{VPM} dataset (VPM GPP V20) used different ε_0 values for C3 and C4 vegetation (Zhang et al., 2017). In VPM model simulations, MODIS-based EVI and NCEP reanalysis climate data were used. When compared with GOME-2 SIF, the 500-m GPP_{VPM} datasets were aggregated from 8-day to monthly and to 0.5° (latitude and longitude).

$$GPP_{VPM} = \varepsilon_{g\times} FPAR_{chl} \times PAR \tag{5}$$

$$\varepsilon_g = \varepsilon_0 \times T_{scalar} \times W_{scalar} \tag{6}$$

where ε_g is light use efficiency, $FPAR_{chl}$ is the fraction of PAR absorbed by chlorophyll, and PAR is the photosynthetic active radiation. GPP_{VPM} uses EVI to estimate $FPAR_{chl}$ and ε_g is estimated using maximum light

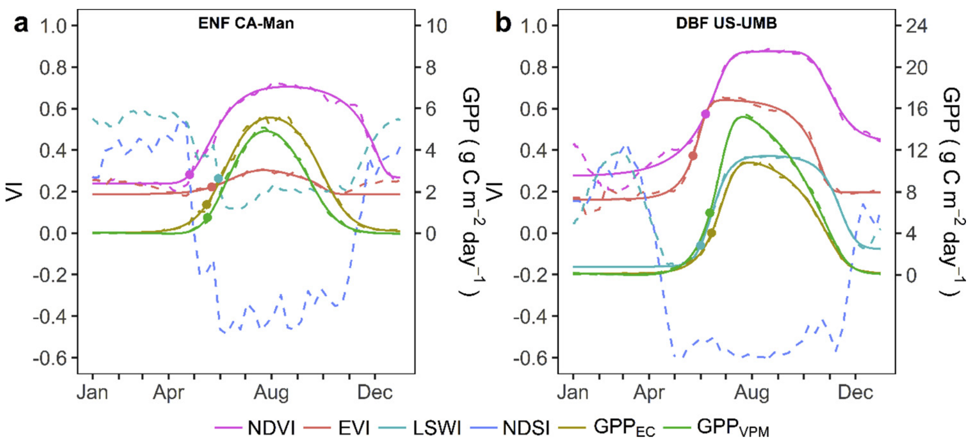

Fig. 2. Seasonal dynamics of MODIS-based vegetation indices (NDSI, NDVI, EVI, LSWI), GPP_{EC}, and GPP_{VPM} at the CA-Man (ENF) site and US-UMB (DBF) site. The curve values are mean values of snow-covered years at each site at 8-day temporal resolution. The dashed lines are original data sets, the solid lines are fitted lines based on double logistic model. Figures for the other ENF and DBF eddy flux tower sites can be found in Fig. S.2 and Fig. S.3. The circle points represent the start of the growing season (SOS) dates estimated from the NDVI, EVI, LSWI and GPP data sources.

use efficiency (ε_0) downregulated by temperature (T_{scalar}) and water stress (W_{scalar}).

2.2.4. GOME-2 SIF data

We used sun-induced chlorophyll fluorescence (SIF) retrievals from the MetOp-A satellite. The GOME-2 MetOp-A satellite has an overpass about 9:30 local solar time and SIF values were retrieved at about 740 nm (Joiner et al., 2013). The GOME-2 instruments have a footprint of about 40 km × 80 km before July 2013, and a 40 km × 40 km footprint after July 2013. We used the GOME-2 SIF V27 level 3 product from 2007 to 2014 at a spatial resolution of 0.5° × 0.5° and monthly resolution.

2.2.5. Land cover data

We used the MODIS land cover dataset (MCD12C1 V051 yearly 0.05°) in 2010 to represent the land cover type (IGBP land cover classification system) throughout the entire study period. We used the majority method to assign the final land cover type when we aggregated the land cover data from 0.05° to 0.5° resolution. Based on MODIS NDSI distribution and land cover data, the snow-covered ENF and DBF pixels were identified at northern mid- to high-latitude regions (30 °N-90 °N) (Fig. 1 b). Then, we calculated monthly and average NDVI, EVI, LSWI, GPP_{VPM}, and SIF for all snow-covered ENF and DBF pixels from 0.5° VIs, GPP_{VPM}, and SIF for each year during 2007 to 2016. Then, SOS dates of snow-covered ENF and DBF across the entire mid- to high-latitude NH were estimated based on the monthly VIs, GPP_{VPM}, and SIF time series.

2.2.6. NCEP temperature data

Daytime temperature data from the National Centers for Environmental Prediction (NCEP) reanalysis project was used in this study. The 6 -hour air temperature at 2 m were downloaded (https://www.esrl.noaa.gov/psd/data/reanalysis/reanalysis.shtml) and daily daytime mean temperature was calculated (Zhang et al., 2017). The original NCEP air temperature products were in the 2.5° x 2.5° global grid (144 × 73). To compare with GPP_{VPM} and SIF, NCEP daily daytime temperatures were composited into monthly data and downscaled to 0.5° spatial resolution using the nearest neighbor method.

2.3. Phenology algorithms

The logistic growth model has been widely used in numerous studies of phenology (Fisher et al., 2006; Gu et al., 2003; Zhang et al., 2003). The 8-day 500 m and monthly 0.5° datasets were interpolated to daily before utilizing logistic regression. We used an improved double logistic growth model (Eq. 7) to estimate vegetation phenology metrics from NDVI, EVI, DBF LSWI, GPP, and SIF datasets (Elmore et al., 2012):

$$A(t) = y_0 + \frac{a_1}{\left[(1+\exp(-\frac{t-t_{01}}{b_1})\right]^{c_1}} + \frac{a_2}{\left[(1+\exp(-\frac{t-t_{02}}{b_2}))\right]^{c_2}} \tag{7}$$

where $A(t)$ is the observation on day t, and y_0, a_1, a_2, b_1, b_2, c_1, c_2, t_{01} and t_{02} are the model parameters to be estimated from the original given data. Start of the growing season (SOS) was calculated using the DOY at the maximum values of the second derivatives (Bucha and Koren, 2017).

LSWI in snow-covered ENF has no significant increase during the growing season, thus it cannot easily be detected by the traditional logistic algorithm. The specific threshold method described in previous studies (Kang et al., 2016; Xiao et al., 2006) was used to determine SOS by LSWI at ENF. In the current study, SOS_{LSWI} of ENF was defined as the first day during the snow-melt period (LSWI decrease period) when LSWI equaled to or lower than 0.3.

3. Results

3.1. Consistency of spring phenology of snow-covered forests at the eddy flux tower sites

The ENF CA-Man site was selected as an example to show the seasonal dynamics of GPP_{EC}, GPP_{VPM}, NDVI, EVI, and LSWI at the snow-covered ENF sites (Fig. 2 a). GPP estimates from the ENF eddy covariance tower (GPP_{EC}) and GPP_{VPM} had a similar seasonal cycle. Both GPP_{EC} and GPP_{VPM} at CA-Man site increased rapidly in late May. SOS dates from GPP_{EC} ($SOS_{GPP\text{-}EC}$) and GPP_{VPM} ($SOS_{GPP\text{-}VPM}$) were identified as 136 and 137 day of year (DOY), respectively. However, NDVI sharply increased in late-April (SOS_{NDVI} was 116 DOY) and EVI started to sharply increase in late-May (SOS_{EVI} was 142 DOY). LSWI was high and peaked at about 0.6 during winter and early spring because of snow cover (NDSI > 0.4), but rapidly decreased in early April due to snowmelt. NDVI was affected by land surface snow cover conditions. When LSWI increased or decreased during the snow cover and snow melting period from winter to early spring, NDVI also decreased or increased. The seasonal dynamics of the other ENF sites had similar results with the CA-Man site; see Fig. S.2 for more information.

The DBF US-UMB site was used as an example to illustrate the seasonal cycles of various variables in the snow-covered DBF sites (Fig. 2 b). Both GPP_{EC} and GPP_{VPM} sharply increased in mid-June, and SOS dates from GPP_{EC} and GPP_{VPM} were 165 and 163 DOY. NDVI showed the first sharp increase in March along with the sharp decrease of LSWI. The dynamics of NDVI also was distinctly converse with those in LSWI curves during the snow cover (NDSI > 0.4) and snowmelt periods (when NDSI decreased from the maximum value) from winter to early spring. EVI and LSWI showed sharp increases in late May, which was consistent with both GPP_{EC} and GPP_{VPM}. For similar seasonal dynamics of the other DBF sites, see Fig. S.3.

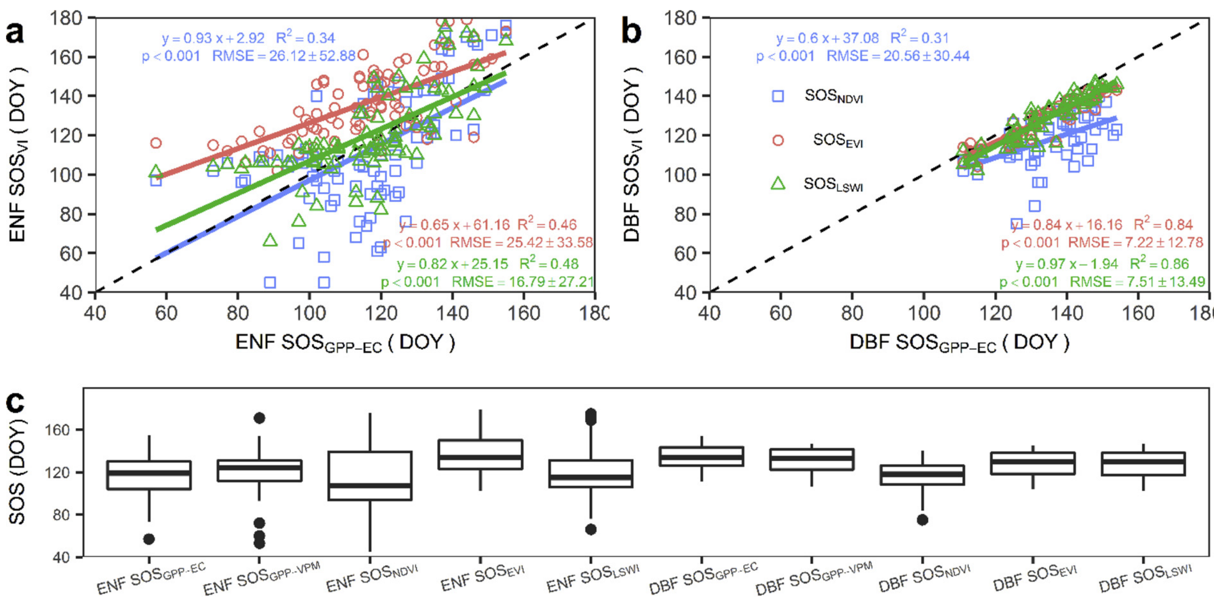

Fig. 3. Comparison of the Start of Growing Season (SOS) dates from NDVI, EVI, LSWI and GPP_{EC} for all snow-covered sites-years: (a) linear regression analyses for ENF, (b) linear regression analysis for DBF, (c) Box plot analysis.

Linear regression analyses for all the snow-covered ENF sites (Fig. 3a) showed that SOS dates estimated by NDVI (SOS_{NDVI}), EVI (SOS_{EVI}), and LSWI (SOS_{LSWI}) were significantly correlated with SOS dates by GPP_{EC} ($SOS_{GPP\text{-}EC}$) ($p < 0.01$). However, their RMSE and R^2 values varied among these three vegetation indices. SOS_{NDVI} had the largest RMSE value (RMSE = 26 ± 53 days) and lowest R^2 ($R^2 = 0.34$) value among the three vegetation indices, while LSWI had smallest RMSE (RMSE = 17 ± 27 days) and highest R^2 ($R^2 = 0.48$) values. Among all the site-years (Fig. 3c), about 50% of $SOS_{GPP\text{-}EC}$ occurred in the range of 104–130 day of year (DOY). The range of SOS_{LSWI} (106–131 DOY) was closer to $SOS_{GPP\text{-}EC}$ than the other two greenness-related vegetation indices: SOS_{NDVI} (94–139 DOY) and SOS_{EVI} (123–150 DOY).

Linear regression analyses for all the snow-covered DBF sites (Fig. 3b) also showed that SOS dates estimated by vegetation indices (SOS_{NDVI}, SOS_{EVI}, and SOS_{LSWI}) were significantly correlated with $SOS_{GPP\text{-}EC}$ ($p < 0.01$) (Fig. 3 b). Both SOS_{EVI} and SOS_{LSWI} had small RMSE values (˜7 days), while SOS_{NDVI} had a large RMSE value (˜21 days). In addition, R^2 value for the linear regression models between SOS_{EVI} ($R^2 = 0.84$) and SOS_{LSWI} ($R^2 = 0.86$) and $SOS_{GPP\text{-}EC}$ were higher than that for SOS_{NDVI} ($R^2 = 0.31$). Among all the site-years (Fig. 3c), 50% of SOS_{EVI}, SOS_{LSWI} and $SOS_{GPP\text{-}EC}$ were distributed in the time range of 120–140 DOY (Fig. 3 c). SOS_{NDVI} was much earlier than SO_{EVI}, SOS_{LSWI}, and $SOS_{GPP\text{-}EC}$.

3.2. Consistency of spring phenology of snow-covered forests across the northern mid- to high-latitudes at 0.5° (latitude and longitude) spatial resolution

We calculated average NDVI, EVI, LSWI, GPP and SIF over all the snow-covered ENF and DBF gridcells (0.5° gridcells) over the northern mid- to high-latitudes, and they had strong seasonal dynamics over the study period (Fig. 4a,b,c,d). There were strong agreements between SIF and GPP_{VPM} data in terms of seasonal dynamics and interannual variation (Fig. 4b,d), and linear relationships between monthly GPP_{VPM} and SIF (Fig. 4e,f) were significant ($p < 0.001$).

For snow-covered ENF in northern mid- to high-latitudes, SOS_{LSWI} dates were significantly consistent with both $SOS_{GPP\text{-}VPM}$ ($p < 0.01$) (Fig. 5a) and SOS_SIF dates ($p < 0.01$) (Fig.5c), while SOS_{NDVI} and SOS_{EVI} dates had no significant linear correlation with $SOS_{GPP\text{-}VPM}$. RMSE values of SOS_{LSWI} dates to $SOS_{GPP\text{-}VPM}$ and SOS_{SIF} were 20 ± 5 days and 16 ± 3 days, respectively. Similar to our site-level analysis, SOS_{NDVI} dates were much earlier than SOS_{EVI}, SOS_{LSWI}, $SOS_{GPP\text{-}VPM}$, and SOS_{SIF} for snow-covered ENF region. In addition, we found that SOS_{SIF} and $SOS_{GPP\text{-}VPM}$ dates were close to each other (Fig. 5a). The differences between SOS_{SIF} and $SOS_{GPP\text{-}VPM}$ ranged from about 0–8 days. As shown in Fig. 5a, $SOS_{GPP\text{-}VPM}$ was on average 5 ± 3 days earlier than SOS_{SIF}.

For snow-covered DBF in northern mid- to high-latitudes, both SOS_{LSWI} ($p < 0.001$) and SOS_{EVI} ($P < 0.01$) had a significant linear correlation with $SOS_{GPP\text{-}VPM}$ (Fig. 5b). However, there was a higher R^2 value between SOS_{LSWI} and $SOS_{GPP\text{-}VPM}$ ($R^2 = 0.8$) than between SOS_{EVI} and $SOS_{GPP\text{-}VPM}$ ($R^2 = 0.62$). RMSE values between SOS_{LSWI} and SOS_{EVI} and $SOS_{GPP\text{-}VPM}$ were 20 ± 2 days and 15 ± 6 days, respectively. SOS_{LSWI} was consistent with SOS_{SIF} ($P < 0.1$) with a RMSE value of 18 ± 6 days while SOS_{NDVI} and SOS_{EVI} didn't significantly correlate with SOS_{SIF} (Fig. 5d). SOS_{NDVI} was also much earlier than SOS from EVI, LSWI, GPP_{VPM}, and SIF. In addition, $SOS_{GPP\text{-}VPM}$ were also similar to SOS_{SIF} for snow-covered DBF forest. Differences between SOS_{SIF} and $SOS_{GPP\text{-}VPM}$ were about 0 ˜ 7 days (Fig.5 a). On average, $SOS_{GPP\text{-}VPM}$ was 2 ± 3 days earlier than SOS_{SIF} at DBF.

3.3. The effect of air temperature on spring phenology of snow-covered forests at both site and regional scales

For the snow-covered ENF and DBF sites, responses of GPP_{EC}, GPP_{VPM}, NDVI, EVI, and LSWI to average daytime air temperature (TemDT) were analyzed (Fig. 6). ENF GPP_{EC} and GPP_{VPM} had similar dynamics in response to TemDT (Fig. 6a,b), which started to increase at ˜0 °C. ENF NDVI, EVI, and LSWI also increased rapidly at 0 °C (Fig. 6c,d,e). DBF GPP_{EC} and GPP_{VPM} had similar dynamics in response to TemDT (Fig. 6f,g), which started to increase at ˜5 °C. DBF NDVI, EVI, and LSWI also increased rapidly at 5 °C (Fig. 6h,i,*j*). We calculated the average TemDT for various SOS dates in snow-covered ENF and DBF sites (Fig. 6k, Table 2). For ENF sites, average TemDT of the SOS dates from GPP_{EC}, GPP_{VPM} and LSWI were close to each other (˜5 to 6 °C), but higher than that from NDVI and lower than that from EVI (Table 2). For DBF sites, average TemDT of SOS for GPP_{EC}, GPP_{VPM}, EVI, and LSWI were similar (˜12 °C), and higher that from NDVI (9.60 °C ± 4.11) (Table 2).

For the snow-covered ENF and DBF gridcells (0.5°) in northern mid- to high-latitudes, responses of GPP_{VPM}, SIF, NDVI, EVI, and LSWI to TemDT were analyzed (Fig. 7). ENF GPP_{VPM} and SIF had similar

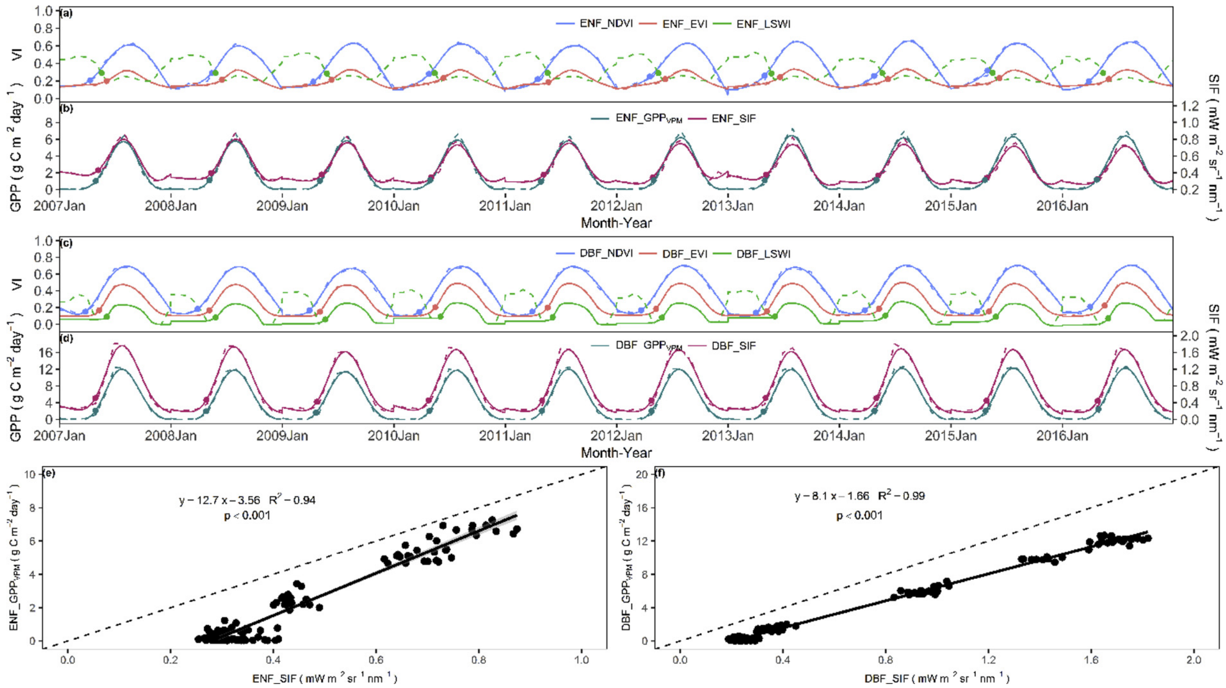

Fig. 4. The seasonal dynamics and interannual variation of average NDVI, EVI, LSWI, GPP_{VPM}, and GOME-2 SIF of all the snow covered ENF (a, b) and DBF (c, d) gridcells (0.5°) as well as the relationships between GPP_{VPM} and SIF for snow-covered ENF (e) and DBF (f) during 2007–2016 in northern mid- to high-latitudes. Points represent the start of the growing season (SOS) for each year.

dynamics in response to TemDT (Fig. 7a,b), starting to increase at ˜5 °C. ENF NDVI, EVI, and LSWI also increased rapidly at 5 °C (Fig. 7c,d,e). DBF GPP_{VPM} and SIF had similar dynamics in response to TemDT (Fig. 7f,g), which started to increase at ˜5 °C. DBF NDVI, EVI and LSWI also increased rapidly at 5 °C (Fig. 7h,i,*j*). We calculated the average TemDT for various SOS dates in snow-covered ENF and DBF gridcells (Fig. 7k, Table 3). For the ENF gridcells, average TemDT of the SOS dates from GPP_{VPM}, SIF and NDVI were close to each other (˜3 to 4 °C), but lower than those from EVI and LSWI (Table 3). For the DBF gridcells, average TemDT of SOS for GPP_{VPM} and SIF were similar (˜6 °C), but higher than NDVI (˜3 °C) and lower than EVI and LSWI (Table 3).

4. Discussion

4.1. The limitations of greenness-related vegetation indices for identifying spring phenology (SOS) of snow-covered forests

Greenness-related vegetation indices (NDVI and EVI) have been used to monitor the spring phenology of ENF (Hmimina et al., 2013; Peng et al., 2017a; Shen et al., 2014a). A previous study found that MODIS NDVI is not an accurate indicator of phenology in evergreen forest in France because MODIS NDVI had smaller values than in-situ NDVI (Hmimina et al., 2013). Two additional studies reported that the lag between ENF SOS_{EVI} and $SOS_{GPP\text{-}EC}$ was about 40–60 days for the United States, and thus EVI can also not be used for accurate SOS estimation (Peng et al., 2017a; Shen et al., 2014a). Consistent with previous studies, our study showed that SOS_{NDVI} and SOS_{EVI} were about 3–4 weeks different from $SOS_{GPP\text{-}EC}$ at the snow-covered ENF sites. The inconsistency of canopy greenness and canopy photosynthesis for snow-covered ENF is due to the fact that the start of photosynthesis in ENF relies on temperature and water availability rather than the emergence and growth new leaves (canopy structural development) (Ensminger et al., 2004; Melaas et al., 2013; Monson et al., 2005).

Many studies suggested that both NDVI (Wu et al., 2017) and EVI (Shen et al., 2014a) can provide an accurate estimation of spring phenology in DBF. For example, Peng et al. (2017a) showed that DBF SOS detected from NDVI and EVI were different from SOS_{GPP} by about 12 days in the United States. However, our study found that NDVI cannot detect SOS in DBF under snow-covered conditions accurately. SOS_{NDVI} in our study had the lowest R square and highest RMSE among these three vegetation indices when compared with $SOS_{GPP\text{-}EC}$ in snow-covered DBF. SOS_{NDVI} was about 3–4 weeks earlier than $SOS_{GPP\text{-}EC}$. Earlier experiments in the snow-covered region of the Northern Hemisphere have shown that both snowmelt and vegetation growth can increase NDVI values (Moulin et al., 1997). Consequently, spring phenology derived from NDVI is always biased due to the snowmelt process, and earlier NDVI increases could be due either to earlier vegetation growth or to earlier snowmelt (Delbart et al., 2005; Huete et al., 2002). Our results indicated that removing snow effects from NDVI signals is of great importance for accurate phenology characterization in snow covered forest regions, even for DBF. So far, some studies have tried to develop thresholds for removing the effects of snow from NDVI time-series data. For example, Suzuki et al. (2003) assumed that snow will not exist when NOAA NDVI exceeds 0.2, while Gamon et al. (2013) suggested that the land surface was snow-free when MODIS NDVI reached 0.3. However, we found that MODIS NDVI was above 0.2 for the whole year at the snow-covered DBF sites, and snow was not completely melted at NDVI value of 0.3 as LSWI was decreasing dramatically (Fig. 1 b). Our research indicated that new approaches for accurate estimates of spring phenology of snow-covered forests are required.

4.2. The potential of water-related vegetation index for identifying spring phenology (SOS) of snow-covered forests

From both the site-level and regional analysis, we found that SOS_{LSWI} was closer to SOS_{GPP} and SOS_{SIF} for both snow-covered DBF and ENF than SOS_{NDVI} and SOS_{EVI}. Meantime, SOS_{LSWI} had lower RMSE values than SOS_{GPP} and SOS_{SIF}. Our results suggested that SOS from LSWI was mostly consistent with functional SOS dates from GPP and SIF at snow-covered forest, and LSWI could be a good indicator for snow-covered ENF and DBF spring phenology detection when referenced by SOS_{GPP} and SOS_{SIF}. Since LSWI values increase with vegetation growth and decrease with snowmelt, it is able to decouple snowmelt signal

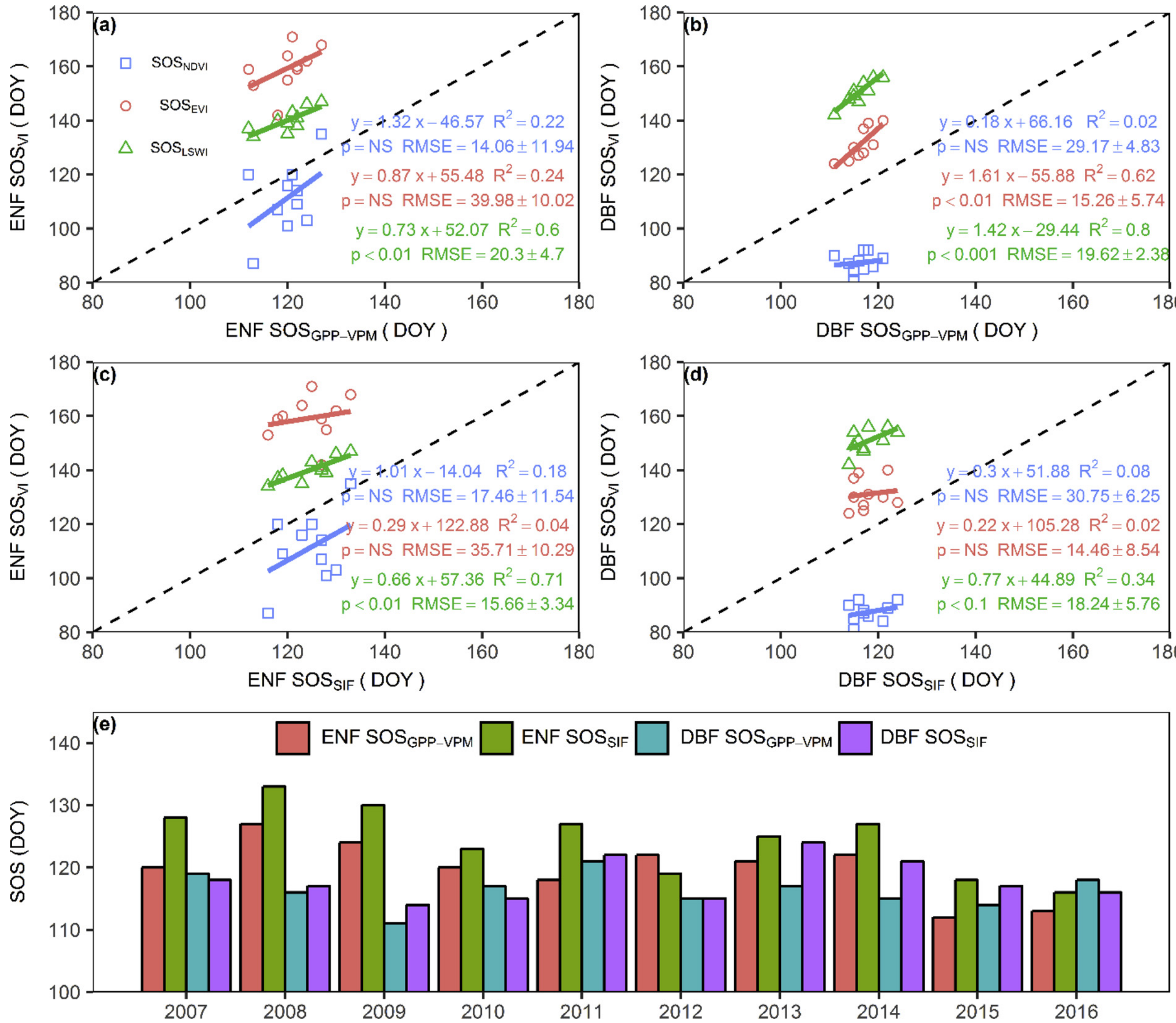

Fig. 5. Comparison of start of growing season (SOS) extracted from NDVI, EVI, LSWI, GPP_{VPM}, and GOME-2 SIF for snow-covered ENF and DBF distributed in northern mid- to high-latitudes during 2007-2016. (a) Comparison of ENF SOS VIs to SOS GPP_{VPM}; (b) Comparison of DBF SOS VIs to SOS GPP_{VPM}; (c) Comparison of ENF SOS VIs to SOS SIF; (d) Comparison of DBF SOS VIs to SOS SIF; (e) Comparison between SOS from GPP_{VPM} and GOME2-SIF of ENF and DBF.

from vegetation growth (Ceccato et al., 2002; Xiao et al., 2009). Some new indices also have been developed using water-related spectral bands and have shown promise for improving the detection of phenology in snow-covered regions (Delbart et al., 2005; Wang et al., 2017). For example, the Normalized Difference Water Index (NDWI), calculated with the near-infrared band (0.78–0.89 μm) and short-wave infrared band (1.58–1.75 μm) from SPOT-VGT, was used for spring phenology detection (Delbart et al., 2005, 2006). The results showed that NDWI can provide better estimations of the start of green-up than NDVI in Eurasia when compared with in-situ phenological records. SPOT-VGT NDWI has also been used in northeastern China for identifying the start and end of the growing season of evergreen forest (Xiao et al., 2002). Normalized Difference Infrared Index (NDII) was calculated from the red band and short-wave infrared band and reflected canopy water content effectively (Hardisky et al., 1983). MODIS NDII was found to be more efficient in estimating the date of onset of greening than methods based on NDVI throughout the central and northern Rocky Mountains of the United States and Canada (Dunn and de Beurs, 2011). Wang et al. (2017) developed a new index named Normalized Difference Phenology Index (NDPI) using three bands of MODIS: near-infrared band, red band, and short-wave infrared band. Analysis at 11 eddy-covariance tower sites in snow-covered deciduous ecosystems showed that NDPI was more reliable than NDVI for spring phenology detection when compared with spring phenology metrics derived from daily GPP.

However, the ability to monitor phenology using water-related vegetation indices remains limited. The specific threshold method was the most popular method for phenology detection based on water-related vegetation indices. For instance, Kang et al. (2016) defined SOS in Tibetan Plateau as the date when LSWI reached -0.1. The threshold selection is relatively subjective, with different thresholds being set by different researchers and study areas. For the sites in our study, the linear relationship between SOS_{LSWI} and SOS_{GPP-EC} varied significantly among the results from different threshold values (Fig. 8). The results suggest that further study is needed to develop a constant algorithm for characterizing phenology of snow-covered ENF. Also note that the average SOS_{SIF} dates were close to $SOS_{GPP-VPM}$, but relatively far away from SOS_{NDVI}, SOS_{EVI} and SOS_{LSWI} (Table 3), which clearly suggested that at the coarse spatial resolution (0.5° in this study) vegetation index data are not appropriate for identifying spring photosynthesis phenology of snow-covered ENF and DBF, because of mixed land cover types within the grid cells. It is more reasonable to characterize spring phenology with time series image data at moderate to high spatial resolutions (e.g., MODIS 500-m; see Table 2).

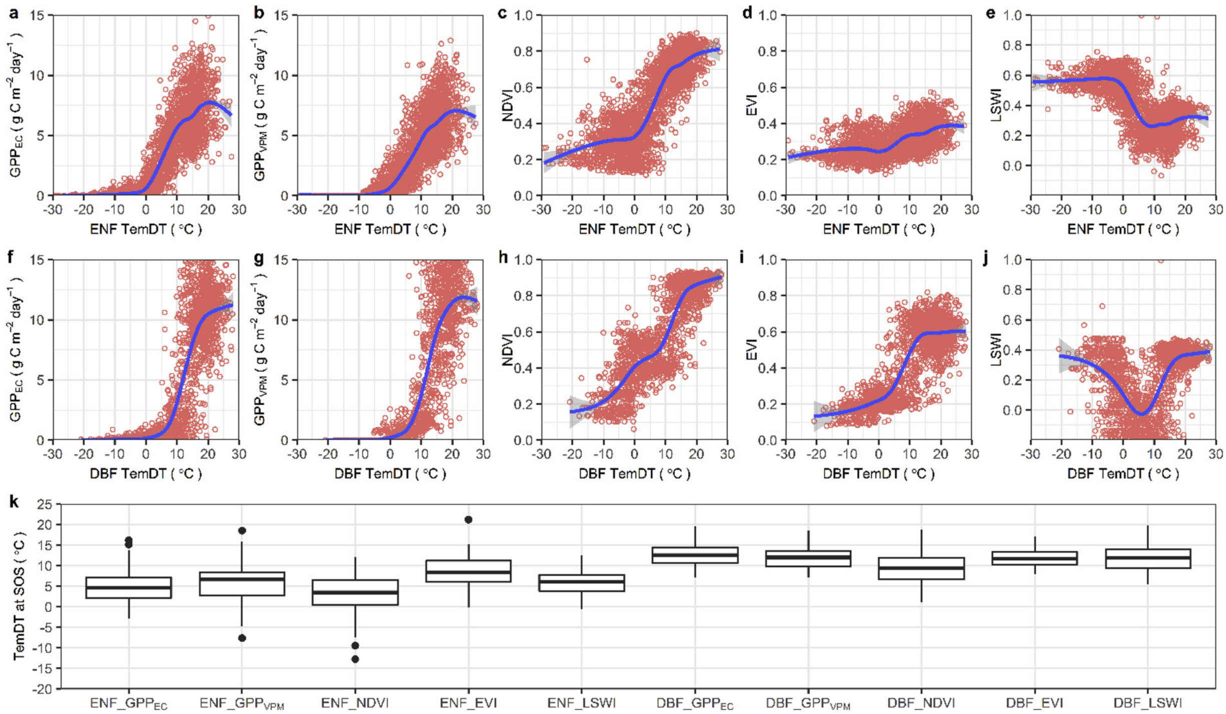

Fig. 6. Relationships between daytime temperature (TemDT) and GPP_{EC}, GPP_{VPM}, NDVI, EVI, and LSWI at ENF and DBF snow-covered sites. All the data during January - August (8-day interval) were used. (a) - (e) are relationships to daytime mean temperature at ENF; (f)-(j) are relationships to daytime mean temperature for DBF. The smooth curves represent the dynamic trends of samples, which were derived from the cyclic penalized cubic regression spline smooth model in R Studio. (k) average TemDT of those SOS dates.

4.3. The role of air temperature for identifying spring phenology (SOS) of snow-covered forests

Air temperature analysis at the time when SOS occurs provides strong evidence for snow-cover conditions in different forest ecosystems. As indicated by GPP_{EC}, photosynthesis at snow-covered ENF sites started at about 5 °C daytime temperature when snow has not yet completely melted (Table 2). Our results match the previous conclusions that the photosynthetic spring recovery in ENF (north of 50 °N) occurs as soon as daily mean temperature temperatures exceed 2–3 °C (Walther et al., 2016). In addition, air temperature is an important factor that directly affects photosynthesis and has been widely used in land surface phenology models (Richardson et al., 2006; Wu et al., 2012). The minimum daily mean temperature for the growth of trees in cold environments was determined to be about 5 °C in the commonly used accumulate temperature phenology model (Prentice et al., 1992). So, our results match the previous assumptions and conclusions in land surface phenology models that are based on temperature. Since evergreen trees do not need to sprout new leaves prior to each growing season, photosynthesis rapidly increases as soon as the required minimum air temperature shows (5 °C), and thus we detected SOS at this time point for ENF. However, we should note that daytime temperature was used in our study, which was different from the above-mentioned phenology models with daily mean temperature. As our results detected ENF SOS_GPP (Table 2) and SOS_SIF (Table 3) at about 5 °C daytime temperature, the daytime temperature is an important factor for plant growth. Piao et al. (2015) also suggested that leaf onset in the northern hemisphere was triggered more by daytime temperature than nighttime temperature and daily mean temperature based on both satellite and in-situ observation datasets. Using daytime temperature instead of daily mean temperature in future land surface phenology models can make the models more reliable.

Even though the minimum air temperature for tree growth is 5 °C, we detected DBF SOS at about 12 °C when snow has melted completely (He et al., 2014), because unlike ENF, DBF photosynthesis in the spring relies on new leaves. Basically, the SOS we detected in DBF was the time when new leaves expanded rapidly. When air temperature reaches the minimum required for growth (5 °C), buds start to develop. After that, it takes some days to accumulate temperature so that the buds can expand into leaves in DBF. For example, in-situ observation in North America found that the progression from bud swelling noticeably to 75% leaves expanded takes about 24 calendar days for tree species (Richardson et al., 2006). Obviously, temperature requirements for SOS in ENF and DBF are completely different. However, temperature conditions were set as the same for SOS measurement in both ENF and DBF in previous studies. For example, SOS was always defined as the time when degree-days above 5 °C had accumulated to at least 40 for all kinds of land cover types in previous studies (Liu et al., 2016; Wu et al.,

Table 2
Average and standard deviation of SOS measured by GPP_{EC} and GPP_{VPM} for the snow-covered ENF and DBF sites (500-m), and average daytime air temperature (TemDT) of those SOS dates.

ENF	ENF GPP_{EC}	ENF GPP_{VPM}	ENF NDVI	ENF EVI	ENF LSWI
SOS (DOY)	117 ± 20	121 ± 18	112 ± 32	136 ± 18	120 ± 22
TemDT at SOS (°C)	4.9 ± 3.71	6.01 ± 4.98	3.02 ± 4.69	8.65 ± 3.65	5.82 ± 2.87
DBF	DBF GPP_{EC}	DBF GPP_{VPM}	DBF NDVI	DBF EVI	DBF LSWI
SOS (DOY)	134 ± 12	130 ± 12	117 ± 13	128 ± 11	128 ± 12
TemDT at SOS (°C)	12.76 ± 2.96	12.07 ± 2.66	9.60 ± 4.11	11.91 ± 2.36	11.86 ± 3.04

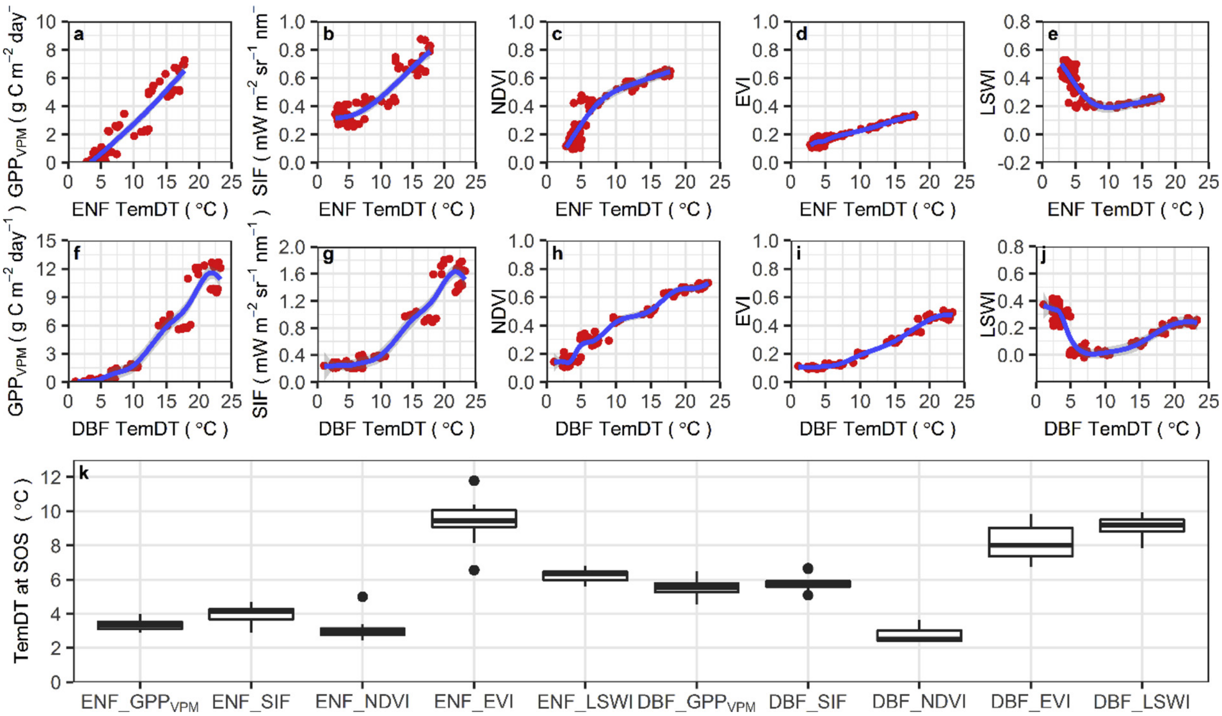

Fig. 7. Response of GPP_{VPM}, GOME-2 SIF, NDVI, EVI, and LSWI to average daytime air temperature gradient (TemDT) over the snow-covered ENF and DBF gridcells (0.5°) in northern mid- to high latitudes (Fig. 1). (a) - (e) ENF gridcells; (f)-(j) DBF gridcells, (k) average TemDT of tjhose SOS dates.

Table 3
Average and standard deviation of SOS dates measured by GPP_{VPM} and SIF for the snow-covered ENF and DBF gridcells (0.5°) in northern mid- to high-latitudes (Fig. 1), and average daytime air temperature (TemDT) of those SOS dates.

ENF	ENF GPP_{vpm}	ENF SIF	ENF NDVI	ENF EVI	ENF LSWI
SOS (DOY)	120 ± 5	125 ± 6	111 ± 13	159 ± 8	140 ± 4
TemDT at SOS (°C)	3.37 ± 0.35	3.93 ± 0.58	3.13 ± 0.71	9.39 ± 1.39	6.27 ± 0.41
DBF	DBF GPP_{vpm}	DBF SIF	DBF NDVI	DBF EVI	DBF LSWI
SOS (DOY)	116 ± 3	118 ± 3.35	87 ± 4	131 ± 6	136 ± 4
TemDT at SOS (°C)	5.54 ± 0.54	5.78 ± 5.24	2.75 ± 0.44	8.14 ± 1.05	9.11 ± 0.6

2012). Based on the same temperature model, the results showed that growing season length based on accumulate temperature model was less consistent with carbon uptake length in ENF and mixed forest than DBF (Wu et al., 2012). Thus, future phenology models with temperature which developed respectively for various land cover types are necessary.

4.4. The contribution of comparing spring phenology from NDVI, EVI, LSWI, and GPP with SOS SIF

Our study provided a comprehensive comparison among SOS dates from NDVI, EVI, GPP_{VPM}, and SIF for the snow-covered ENF and DBF region in mid- to high-latitude Northern Hemisphere. SIF has recently been used for exploring land surface ecosystem seasonal dynamics in several studies (Jeong et al., 2017; Walther et al., 2016). Jeong et al. (2017) used GOME-2 SIF data to examine physiological activity over northern high-latitude forests (40°–55 °N), and their results indicated a large-scale seasonal decoupling of structural growing season length from NDVI and physiological growing growth season length from SIF (by about 46 days). Walther et al. (2016) also found that MODIS GPP and SIF showed similar seasonality in both ENF and DBF ecosystems in the northern hemisphere, and photosynthesis SOS indicated by SIF is about 1 month earlier than canopy greenness SOS indicated by EVI in ENF. Consistent with previous studies, we also found $SOS_{GPP\text{-}VPM}$ and SOS_{SIF} air temperature to be similar. Quantitatively, our study concluded that difference between the dates of $SOS_{GPP\text{-}VPM}$ and SOS_{SIF} is about 5 ± 3 days for snow-covered ENF and 2 ± 3 days for snow-covered DBF in the mid- to high-latitude NH, which can be a good reference for future phenology studies. Our study found that SOS from NDVI and EVI was not significantly correlated with SOS from GOME-2 SIF for snow-covered ENF and DBF sites (Fig. 6c,d). SOS from the water-related vegetation index (LSWI) were found to be most consistent with $SOS_{GPP\text{-}VPM}$ and SOS_{SIF} for snow-covered ENF and DBF for the first time. In addition, SOS_{NDVI} dates were earlier than the structural phenology of SOS_{EVI} and SOS_{LSWI}, as well as earlier than the functional phenology of $SOS_{GPP\text{-}VPM}$ and SOS_{SIF}. Our conclusions for regional analysis were consistent with the conclusions for sites analysis.

However, we should note that when exploring the consistency between SOS from satellite-based GPP and SIF is that GPP and SIF represent the fate of absorbed PAR at different time scales. We used instantaneous GOME-2 SIF measurements while GPP_{VPM} simulates daily average rate of photosynthesis every 8 days. Even though daily SIF products have been developed using instantaneous SIF observations and have a better consistency with daily GPP (Joiner et al., 2013; Zhang et al., 2018), the robustness of the results will be affected by the quality of the model used to calculate daily SIF and the interpolation of 8-day GPP to daily values. In addition, the SIF data is especially noisy and there are less frequent measurements in some regions (Joiner et al., 2012). It is critical that future studies utilize SIF and reflectance data with high spatial and temporal resolution so that we can reach a greater understanding about the phenology worldwide.

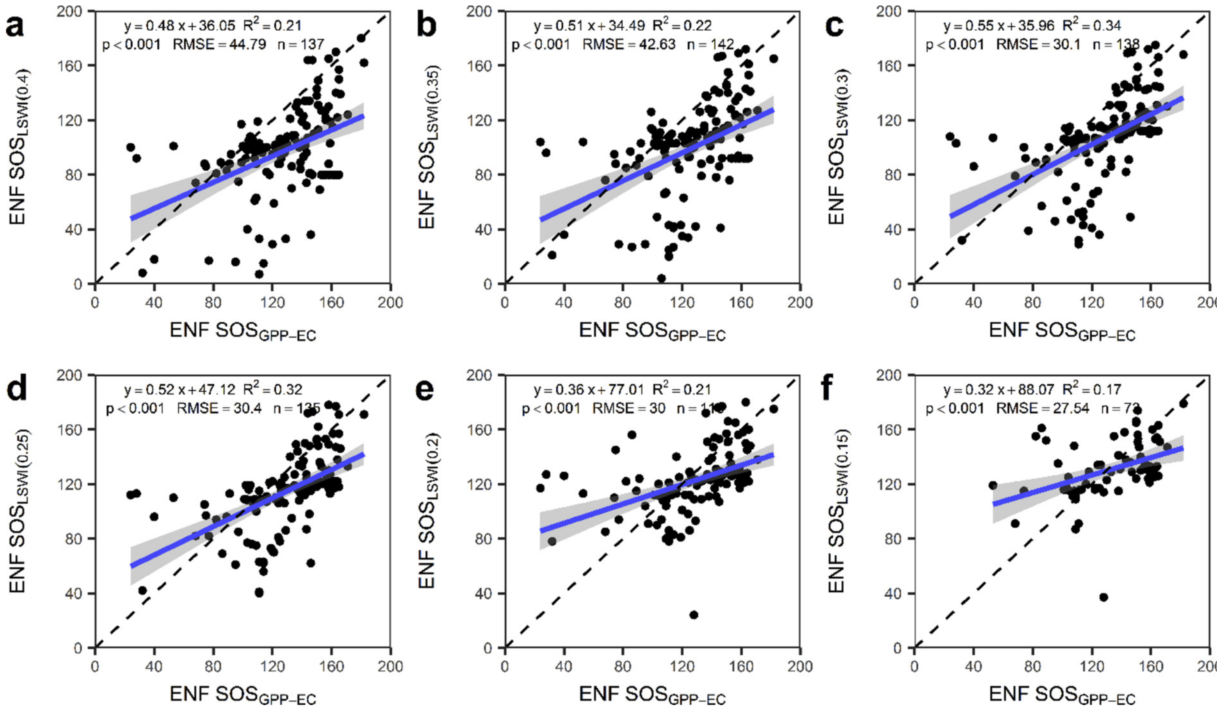

Fig. 8. Relationship between SOS extracted with different threshold values of LSWI (ENF SOS_LSWI$_{threshold}$) and SOS extracted from eddy covariance GPP (ENF SOS$_{GPP\text{-}EC}$) at snow-covered ENF eddy covariance sites. The threshold values were selected from 0.4 to 0.15, with 0.05 decreasing interval (0.4, 0.35, 0.3, 0.25, 0.2, 0.15).

5. Conclusions

Snow cover and snowmelt affect land surface reflectance leading to bias SOS estimates in snow-covered forests. We comprehensively compared the consistency of SOS dates derived from MODIS vegetation indices (NDVI, EVI, LSWI), GPP_{EC}, GPP_{VPM}, and GOME-2 SIF for snow-covered DBF and ENF ecosystems. In addition, we analyzed daytime air temperature so that we can not only better understand when snowmelt and SOS occur in various datasets but also evaluate the reliability of SOS results from various datasets. Based on our analysis, comparison of estimated SOS dates, and the relationship between SOS and air temperature, we found that VIs (NDVI, EVI, and LSWI) performed differently in snow-covered ENF and DBF ecosystems. Furthermore, GPP_{VPM} was significantly correlated with SIF, and thus canopy functional SOS detected from the two datasets were similar. Our results highlight that the remote-sensing of phenology at higher latitudes needs further development to account for the impacts of snow cover on greenness-related vegetation indices (NDVI and EVI). We suggest SOS estimates should make full use of water-related vegetation indices and consider daytime air temperature so that we may better understand the relationship between the changes in greenness and photosynthesis.

Acknowledgements

This study was supported by research grants from USDA National Institute of Food and Agriculture (NIFA) (2013-69002 and 2016-68002-24967), the US National Science Foundation EPSCoR program (IIA-1301789), and NASA Geostationary Carbon Cycle Observatory mission (GeoCarb Contract #80LARC17C0001). This work used eddy covariance data acquired and shared by the FLUXNET community, including these networks: AmeriFlux, AfriFlux, AsiaFlux, CarboAfrica, CarboEuropeIP, CarboItaly, CarboMont, ChinaFlux, Fluxnet-Canada, GreenGrass, ICOS, KoFlux, LBA, NECC, OzFlux-TERN, TCOS-Siberia, and USCCC.

Appendix A. Supplementary data

Supplementary material related to this article can be found, in the online version, at doi:https://doi.org/10.1016/j.agrformet.2019.06.002.

References

Baldocchi, D., et al., 2001. FLUXNET: a new tool to study the temporal and spatial variability of ecosystem–scale carbon dioxide, water vapor, and energy flux densities. Bull. Am. Meteorol. Soc. 82 (11), 2415–2434.

Balzarolo, M., et al., 2016. Matching the phenology of net ecosystem exchange and vegetation indices estimated with MODIS and FLUXNET in-situ observations. Remote Sens. Environ. 174, 290–300.

Botta, A., Viovy, N., Ciais, P., Friedlingstein, P., Monfray, P., 2000. A global prognostic scheme of leaf onset using satellite data. Glob. Chang. Biol. 6 (7), 709–725.

Bucha, T., Koren, M., 2017. Phenology of the beech forests in the Western Carpathians from MODIS for 2000-2015. iForest-Biogeosciences and Forestry 10 (3), 537.

Ceccato, P., Flasse, S., Gregoire, J.-M., 2002. Designing a spectral index to estimate vegetation water content from remote sensing data: part 2. Validation and applications. Remote Sens. Environ. 82 (2-3), 198–207.

Chang, Q., Zhang, J., Jiao, W., Yao, F., 2018. A comparative analysis of the NDVIg and NDVI3g in monitoring vegetation phenology changes in the Northern Hemisphere. Geocarto Int. 33 (1), 1–20.

Chen, J., et al., 2004. A simple method for reconstructing a high-quality NDVI time-series data set based on the Savitzky–Golay filter. Remote Sens. Environ. 91 (3-4), 332–344.

Chen, X., Liang, S., Cao, Y., He, T., Wang, D., 2015. Observed contrast changes in snow cover phenology in northern middle and high latitudes from 2001–2014. Sci. Rep. 5, 16820.

Churkina, G., Schimel, D., Braswell, B.H., Xiao, X., 2005. Spatial analysis of growing season length control over net ecosystem exchange. Glob. Chang. Biol. 11 (10), 1777–1787.

Delbart, N., Kergoat, L., Le Toan, T., Lhermitte, J., Picard, G., 2005. Determination of phenological dates in boreal regions using normalized difference water index. Remote Sens. Environ. 97 (1), 26–38.

Delbart, N., Le Toan, T., Kergoat, L., Fedotova, V., 2006. Remote sensing of spring phenology in boreal regions: a free of snow-effect method using NOAA-AVHRR and SPOT-VGT data (1982–2004). Remote Sens. Environ. 101 (1), 52–62.

Dunn, A.H., de Beurs, K.M., 2011. Land surface phenology of North American mountain environments using moderate resolution imaging spectroradiometer data. Remote Sens. Environ. 115 (5), 1220–1233.

Elmore, A.J., Guinn, S.M., Minsley, B.J., Richardson, A.D., 2012. Landscape controls on the timing of spring, autumn, and growing season length in mid-Atlantic forests. Glob. Chang. Biol. 18 (2), 656–674.

Ensminger, I., et al., 2004. Intermittent low temperatures constrain spring recovery of photosynthesis in boreal Scots pine forests. Glob. Chang. Biol. 10 (6), 995–1008.
Fisher, J.I., Mustard, J.F., Vadeboncoeur, M.A., 2006. Green leaf phenology at Landsat resolution: scaling from the field to the satellite. Remote Sens. Environ. 100 (2), 265–279.
Gamon, J.A., Huemmrich, K.F., Stone, R.S., Tweedie, C.E., 2013. Spatial and temporal variation in primary productivity (NDVI) of coastal Alaskan tundra: Decreased vegetation growth following earlier snowmelt. Remote Sens. Environ. 129, 144–153.
Garrity, S.R., et al., 2011. A comparison of multiple phenology data sources for estimating seasonal transitions in deciduous forest carbon exchange. Agric. For. Meteorol. 151 (12), 1741–1752.
Groendahl, L., Friborg, T., Søgaard, H., 2007. Temperature and snow-melt controls on interannual variability in carbon exchange in the high Arctic. Theor. Appl. Climatol. 88 (1-2), 111–125.
Gu, L., et al., 2003. Phenology of vegetation photosynthesis. Phenology: An integrative environmental science. pp. 467–485.
Guanter, L., et al., 2014. Global and time-resolved monitoring of crop photosynthesis with chlorophyll fluorescence. Proc. Natl. Acad. Sci. 111 (14), E1327–E1333.
Hall, D.K., Riggs, G.A., Salomonson, V.V., 1995. Development of methods for mapping global snow cover using moderate resolution imaging spectroradiometer data. Remote Sens. Environ. 54 (2), 127–140.
Hall, D.K., Riggs, G.A., Salomonson, V.V., DiGirolamo, N.E., Bayr, K.J., 2002. MODIS snow-cover products. Remote Sens. Environ. 83 (1-2), 181–194.
Hardisky, M., Klemas, V., Smart, M., 1983. The influence of soil salinity, growth form, and leaf moisture on the spectral radiance of. Spartina alterniflora 49, 77–83.
He, Z., Parajka, J., Tian, F., Blöschl, G., 2014. Estimating degree-day factors from MODIS for snowmelt runoff modeling. Hydrol. Earth Syst. Sci. 18 (12), 4773–4789.
Hmimina, G., et al., 2013. Evaluation of the potential of MODIS satellite data to predict vegetation phenology in different biomes: an investigation using ground-based NDVI measurements. Remote Sens. Environ. 132, 145–158.
Hollinger, D., et al., 1999. Seasonal patterns and environmental control of carbon dioxide and water vapour exchange in an ecotonal boreal forest. Glob. Chang. Biol. 5 (8), 891–902.
Huete, A., et al., 2002. Overview of the radiometric and biophysical performance of the MODIS vegetation indices. Remote Sens. Environ. 83 (1), 195–213.
Jeong, S.-J., et al., 2017. Application of satellite solar-induced chlorophyll fluorescence to understanding large-scale variations in vegetation phenology and function over northern high latitude forests. Remote Sens. Environ. 190, 178–187.
Joiner, J., et al., 2013. Global monitoring of terrestrial chlorophyll fluorescence from moderate-spectral-resolution near-infrared satellite measurements: methodology, simulations, and application to GOME-2. Atmos. Meas. Tech. 6 (10), 2803–2823.
Joiner, J., et al., 2012. Filling-in of near-infrared solar lines by terrestrial fluorescence and other geophysical effects: simulations and space-based observations from SCIAMACHY and GOSAT. Atmos. Meas. Tech. 5 (4), 809–829.
Joiner, J., et al., 2014. The seasonal cycle of satellite chlorophyll fluorescence observations and its relationship to vegetation phenology and ecosystem atmosphere carbon exchange. Remote Sens. Environ. 152, 375–391.
Julien, Y., Sobrino, J., 2009. Global land surface phenology trends from GIMMS database. Int. J. Remote Sens. 30 (13), 3495–3513.
Kang, X., et al., 2016. Variability and changes in climate, phenology, and gross primary production of an alpine wetland ecosystem. Remote Sens. (Basel) 8 (5), 391.
Kumar, J., Hoffman, F.M., Hargrove, W.W., Collier, N., 2016. Understanding the Representativeness of FLUXNET for Upscaling Carbon Flux From Eddy Covariance Measurements. 1866-3591. Oak Ridge National Lab.(ORNL), Oak Ridge, TN (United States).
Lasslop, G., et al., 2010. Separation of net ecosystem exchange into assimilation and respiration using a light response curve approach: critical issues and global evaluation. Glob. Chang. Biol. 16 (1), 187–208.
Li, X., et al., 2018. Solar-induced chlorophyll fluorescence is strongly correlated with terrestrial photosynthesis for a wide variety of biomes: First global analysis based on OCO-2 and flux tower observations. Glob. Chang. Biol. 24 (9), 3990–4008.
Liu, Y., et al., 2016. Improved modeling of land surface phenology using MODIS land surface reflectance and temperature at evergreen needleleaf forests of central North America. Remote Sens. Environ. 176, 152–162.
Ma, S., Baldocchi, D.D., Xu, L., Hehn, T., 2007. Inter-annual variability in carbon dioxide exchange of an oak/grass savanna and open grassland in California. Agric. For. Meteorol. 147 (3), 157–171.
Matsumoto, K., Ohta, T., Irasawa, M., Nakamura, T., 2003. Climate change and extension of the Ginkgo biloba L. Growing season in Japan. Glob. Chang. Biol. 9 (11), 1634–1642.
Melaas, E.K., et al., 2013. Using FLUXNET data to improve models of springtime vegetation activity onset in forest ecosystems. Agric. For. Meteorol. 171, 46–56.
Monson, R.K., et al., 2005. Climatic influences on net ecosystem CO 2 exchange during the transition from wintertime carbon source to springtime carbon sink in a high-elevation, subalpine forest. Oecologia 146 (1), 130–147.
Moulin, S., Kergoat, L., Viovy, N., Dedieu, G., 1997. Global-scale assessment of vegetation phenology using NOAA/AVHRR satellite measurements. J. Clim. 10 (6), 1154–1170.
Peng, D., et al., 2017a. Spring green-up phenology products derived from MODIS NDVI and EVI: intercomparison, interpretation and validation using National Phenology Network and AmeriFlux observations. Ecol. Indic. 77, 323–336.
Peng, D., et al., 2017b. Intercomparison and evaluation of spring phenology products using National Phenology Network and AmeriFlux observations in the contiguous United States. Agric. For. Meteorol. 242, 33–46.
Peñuelas, J., Filella, I., 2009. Phenology feedbacks on climate change. Science 324 (5929), 887–888.
Piao, S., Friedlingstein, P., Ciais, P., Viovy, N., Demarty, J., 2007. Growing season extension and its impact on terrestrial carbon cycle in the Northern Hemisphere over the past 2 decades. Global Biogeochem. Cycles 21 (3).
Piao, S., et al., 2015. Leaf onset in the northern hemisphere triggered by daytime temperature. Nat. Commun. 6.
Prentice, I.C., et al., 1992. Special paper: a global biome model based on plant physiology and dominance, soil properties and climate. J. Biogeogr. 117–134.
Reed, B.C., Schwartz, M.D., Xiao, X., 2009. Remote Sensing Phenology, Phenology of Ecosystem Processes. Springer, pp. 231–246.
Richardson, A.D., Bailey, A.S., Denny, E.G., Martin, C.W., O'KEEFE, J., 2006. Phenology of a northern hardwood forest canopy. Glob. Chang. Biol. 12 (7), 1174–1188.
Richardson, A.D., et al., 2010. Influence of spring and autumn phenological transitions on forest ecosystem productivity. Philos. Trans. R. Soc. Lond., B, Biol. Sci. 365 (1555), 3227–3246.
Rouse Jr., J.W., Haas, R., Schell, J., Deering, D., 1974. Monitoring Vegetation Systems in the Great Plains With ERTS.
Savitzky, A., Golay, M.J., 1964. Smoothing and differentiation of data by simplified least squares procedures. Anal. Chem. 36 (8), 1627–1639.
Shen, M., Tang, Y., Desai, A.R., Gough, C., Chen, J., 2014a. Can EVI-derived land-surface phenology be used as a surrogate for phenology of canopy photosynthesis? Int. J. Remote Sens. 35 (3), 1162–1174.
Shen, M.G., et al., 2014b. Increasing altitudinal gradient of spring vegetation phenology during the last decade on the Qinghai-Tibetan Plateau. Agric. For. Meteorol. 189, 71–80.
Sims, D.A., et al., 2006. On the use of MODIS EVI to assess gross primary productivity of North American ecosystems. J. Geophys. Res. Biogeosci. 111 (G4).
Sun, Y., et al., 2018. Overview of Solar-Induced chlorophyll Fluorescence (SIF) from the Orbiting Carbon Observatory-2: retrieval, cross-mission comparison, and global monitoring for GPP. Remote Sens. Environ. 209, 808–823.
Suzuki, R., Nomaki, T., Yasunari, T., 2003. West–east contrast of phenology and climate in northern Asia revealed using a remotely sensed vegetation index. Int. J. Biometeorol. 47 (3), 126–138.
Verma, M., et al., 2014. Remote Sensing of Annual Terrestrial Gross Primary Productivity From MODIS: an Assessment Using the FLUXNET La Thuile Data Set.
Vermote, E., 2015. MOD09A1 MODIS/Terra Surface Reflectance 8-Day L3 Global 500m SIN Grid V006, vol. 10 NASA EOSDIS Land Processes DAAC.
Viovy, N., Arino, O., Belward, A., 1992. The best index slope extraction (BISE): a method for reducing noise in NDVI time-series. Int. J. Remote Sens. 13 (8), 1585–1590.
Walther, S., et al., 2016. Satellite chlorophyll fluorescence measurements reveal large-scale decoupling of photosynthesis and greenness dynamics in boreal evergreen forests. Glob. Chang. Biol. 22 (9), 2979–2996.
Wang, C., Cao, R., Chen, J., Rao, Y., Tang, Y., 2015. Temperature sensitivity of spring vegetation phenology correlates to within-spring warming speed over the Northern Hemisphere. Ecol. Indic. 50, 62–68.
Wang, C., et al., 2017. A snow-free vegetation index for improved monitoring of vegetation spring green-up date in deciduous ecosystems. Remote Sens. Environ. 196, 1–12.
Wang, Y., Tang, X., Yu, L., Hou, X., Munger, J.W., 2016. Comparison of net ecosystem carbon exchange estimation in a mixed temperate forest using field eddy covariance and MODIS data. SpringerPlus 5 (1), 491.
White, M.A., Thornton, P.E., Running, S.W., 1997. A continental phenology model for monitoring vegetation responses to interannual climatic variability. Global Biogeochem. Cycles 11 (2), 217–234.
Wu, C., et al., 2013. Interannual variability of net ecosystem productivity in forests is explained by carbon flux phenology in autumn. Glob. Ecol. Biogeogr. 22 (8), 994–1006.
Wu, C., Gonsamo, A., Gough, C.M., Chen, J.M., Xu, S., 2014. Modeling growing season phenology in North American forests using seasonal mean vegetation indices from MODIS. Remote Sens. Environ. 147, 79–88.
Wu, C., et al., 2017. Land surface phenology derived from normalized difference vegetation index (NDVI) at global FLUXNET sites. Agric. For. Meteorol. 233, 171–182.
Wu, C., et al., 2012. Interannual and spatial impacts of phenological transitions, growing season length, and spring and autumn temperatures on carbon sequestration: a North America flux data synthesis. Glob. Planet. Change 92-93, 179–190.
Xiao, J., et al., 2008. Estimation of net ecosystem carbon exchange for the conterminous United States by combining MODIS and AmeriFlux data. Agric. For. Meteorol. 148 (11), 1827–1847.
Xiao, X., Boles, S., Liu, J., Zhuang, D., Liu, M., 2002. Characterization of forest types in Northeastern China, using multi-temporal SPOT-4 VEGETATION sensor data. Remote Sens. Environ. 82 (2), 335–348.
Xiao, X., Hagen, S., Zhang, Q., Keller, M., Moore, B., 2006. Detecting leaf phenology of seasonally moist tropical forests in South America with multi-temporal MODIS images. Remote Sens. Environ. 103 (4), 465–473.
Xiao, X., et al., 2004a. Satellite-based modeling of gross primary production in an evergreen needleleaf forest. Remote Sens. Environ. 89 (4), 519–534.
Xiao, X., Zhang, J., Yan, H., Wu, W., Biradar, C., 2009. Land Surface Phenology, Phenology of Ecosystem Processes. Springer, pp. 247–270.
Xiao, X., et al., 2004b. Modeling gross primary production of temperate deciduous broadleaf forest using satellite images and climate data. Remote Sens. Environ. 91 (2), 256–270.
Zhang, G.L., Zhang, Y.J., Dong, J.W., Xiao, X.M., 2013. Green-up dates in the Tibetan Plateau have continuously advanced from 1982 to 2011. Proc. Natl. Acad. Sci. U. S. A. 110 (11), 4309–4314.
Zhang, X., 2015. Reconstruction of a complete global time series of daily vegetation index trajectory from long-term AVHRR data. Remote Sens. Environ. 156, 457–472.
Zhang, X., Friedl, M.A., Schaaf, C.B., 2006. Global vegetation phenology from Moderate Resolution Imaging Spectroradiometer (MODIS): evaluation of global patterns and

comparison with in situ measurements. J. Geophys. Res. Biogeosci. 111 (G4).
Zhang, X., et al., 2003. Monitoring vegetation phenology using MODIS. Remote Sens. Environ. 84 (3), 471–475.
Zhang, Y., et al., 2016a. Model-based analysis of the relationship between sun-induced chlorophyll fluorescence and gross primary production for remote sensing applications. Remote Sens. Environ. 187, 145–155.
Zhang, Y., et al., 2016b. Consistency between sun-induced chlorophyll fluorescence and gross primary production of vegetation in North America. Remote Sens. Environ. 183, 154–169.
Zhang, Y., et al., 2017. A global moderate resolution dataset of gross primary production of vegetation for 2000–2016. Sci. Data 4, 170165.
Zhang, Y., et al., 2018. On the relationship between sub-daily instantaneous and daily total gross primary production: implications for interpreting satellite-based SIF retrievals. Remote Sens. Environ. 205, 276–289.